Journal of Marine Systems 78 (2009) 319–326

Contents lists available at ScienceDirect

Journal of Marine Systems

journal homepage: www.elsevier.com/locate/jmarsys

An algorithm for oceanic front detection in chlorophyll and SST satellite imagery

Igor M. Belkin [a,*], John E. O'Reilly [b]

[a] Graduate School of Oceanography, University of Rhode Island, Narragansett, RI 02882, United States
[b] Northeast Fisheries Science Center/Narragansett Laboratory, National Marine Fisheries Service/NOAA, Narragansett, RI 02882, United States

ARTICLE INFO

Article history:
Received 2 September 2007
Received in revised form 12 October 2008
Accepted 7 November 2008
Available online 20 February 2009

Keywords:
Oceanic front
Satellite imagery
Remote sensing
Chlorophyll
SST
Frontal oceanography
Front detection

ABSTRACT

An algorithm is described for oceanic front detection in chlorophyll (Chl) and sea surface temperature (SST) satellite imagery. The algorithm is based on a gradient approach: the main novelty is a shape-preserving, scale-sensitive, contextual median filter applied selectively and iteratively until convergence. This filter has been developed specifically for Chl since these fields have spatial patterns such as chlorophyll enhancement at thermohaline fronts and small- and meso-scale chlorophyll blooms that are not present in SST fields. Linear Chl enhancements and localized (point-wise) blooms are modeled as ridges and peaks respectively, whereas conventional fronts in Chl and SST fields are modeled as steps or ramps. Examples are presented of the algorithm performance using modeled (synthetic) images as well as synoptic Chl and SST imagery. After testing, the algorithm was used on >6000 synoptic images, 1999–2007, to produce climatologies of Chl and SST fronts off the U.S. Northeast.

1. Introduction

The advent of remote sensing from satellites has enabled global monitoring of oceanic fronts from space. The first property used for this purpose was sea surface temperature, SST. In a seminal worldwide survey of oceanic fronts, Legeckis (1978) demonstrated a variety of SST fronts formed by vastly different physical processes — water mass convergences, river outflows, tidal mixing, coastal and open ocean upwelling etc. These processes create sharp horizontal gradients of SST identified with thermal fronts.

Such gradient zones or "edges" can be detected in SST imagery by objective methods. Two approaches became widely accepted: the gradient method thanks mainly to its simplicity (e.g. Kazmin and Rienecker, 1996; Moore et al., 1997, 1999; Kostianoy et al., 2004; Breaker et al., 2005); and the histogram method (Cayula and Cornillon, 1992, 1995, 1996), owing to its robustness and ample worldwide validation (Kahru et al., 1995; Belkin et al., 1998; Ullman and Cornillon, 1999; Ullman and Cornillon, 2000; Hickox et al., 2000; Belkin et al., 2001; Ullman and Cornillon, 2001; Mavor and Bisagni, 2001; Belkin et al., 2003; Belkin and Cornillon, 2003, 2004, 2005; Nieto and Demarcq, 2006; Miller, this issue; Belkin et al., in press). Other methods have been tried as well, notably the Canny (1986) edge detector (e.g. Castelao et al., 2006; Nieto and Demarcq, 2006), the Holyer and Peckinpaugh (1989) cluster-shadow method (e.g. Cayula et al., 1991), and the Vazquez et al. (1999) entropic approach (e.g. Shimada et al., 2005).

Thermal fronts enjoyed much-deserved attention partly because of widely available high-quality global imagery from NOAA satellites (e.g. Pathfinder data set; Vazquez et al., 1998) that extends back to mid-1980s. Oceanic parameters other than SST were not widely available until 1997 when SeaWiFS ocean color imagery became available, ushering in the era of global monitoring of estimated chlorophyll-*a* (Chl) concentration from space. The sheer and ever-increasing volume of color imagery called for objective methods of its analysis; in particular, automatic detection of chlorophyll fronts has been widely recognized as a high-priority task (Chan, 1999; Bontempi and Yoder, 2004; Stegmann and Ullman, 2004; Miller, 2004; Nieto and Demarcq, 2006; Miller, this issue). And yet progress in this direction was limited, especially when compared with automatic detection of SST fronts. The most fundamental reason for this lies in the inherent complexity of Chl field versus SST, with Chl featuring spatial patterns that do not exist in SST, namely *Chl blooms* and *Chl enhancement at thermohaline fronts*.

This fundamental difference between Chl and SST fields is illustrated by two respective conceptual models of a generic front separating shelf and oceanic waters usually called the shelf–slope front, SSF, or shelf break front (Figs. 1–5). A typical SST or Chl front can be modeled as a step function or *ramp* (Fig. 2) since the front is a sharp boundary between two relatively uniform water masses with different temperatures or Chl concentration. This simple structure can be seen in a Chl image of the SSF off the U.S. Northeast in Fig. 3. However, the same front during a different season or year may appear quite differently in Chl field. The most peculiar cross-frontal structure characteristic of Chl field features elevated Chl peaking on – or close to – a respective TS-front. This phenomenon is called *chlorophyll enhancement* (at a hydrographic

* Corresponding author.
E-mail address: ibelkin@gso.uri.edu (I.M. Belkin).

0924-7963/$ – see front matter © 2009 Elsevier B.V. All rights reserved.
doi:10.1016/j.jmarsys.2008.11.018

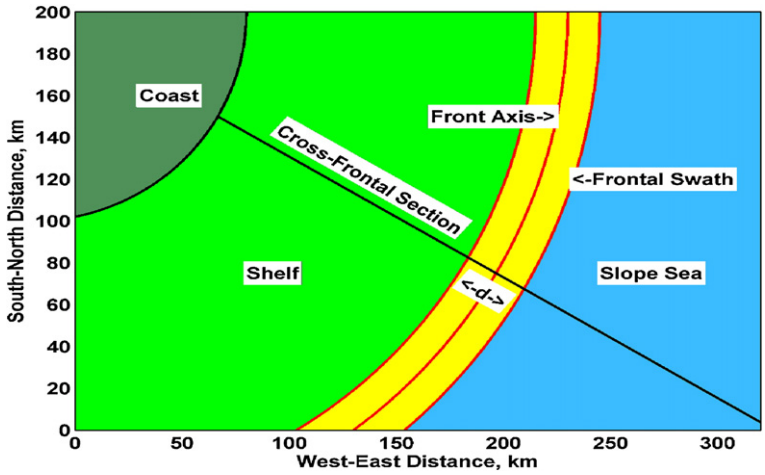

Fig. 1. Plane view of a generic shelf–slope front.

front); its transverse structure can be modeled as a *peak* (Fig. 4). The Chl image of the SSF off the U.S. Northeast in Fig. 5 shows a large-scale Chl enhancement extending over 1000 km along the SSF; similar patterns have been repeatedly observed and extensively studied in this area (Marra et al., 1990; Ryan et al., 1999a,b; Stegmann and Ullman, 2004).

The exact form of the peak model may vary in the above concept that simply illustrates profound differences often observed between SST and Chl patterns in frontal zones. Another important aspect of the Chl field is patchiness on a variety of scales, evident from ocean color imagery and *in situ* data. Spatial structure of Chl field is a product of interplay of physical, chemical, and biological processes, and therefore is inherently more complex than the structure of physical fields such as temperature and salinity. Patchiness is a hallmark of Chl field. It may be formed by physical dynamics, e.g. by the underlying patchiness of the TS-field, and it may also be formed by biological dynamics; it may also result from physical–biological interactions and feedbacks.

The observed richness of spatial patterns and features in the Chl field defies a simplistic approach to front detection based on a single model of cross-frontal transverse structure, be it a step, ramp, peak, or patch. However, there is a common feature associated with the various patterns, which is the *local maximum gradient*. This brings us back to the gradient method and its basic problem: noise. Since every differentiation (gradient computation) results in noise amplification, the noise should be dealt with before front detection/feature extraction. In this work we demonstrate that effective noise suppression combined with feature preservation allows spatial gradients to be computed and mapped in a way that brings out diverse frontal patterns in the Chl field as well as SST fronts.

2. The algorithm and its performance on model images

Our approach to front detection is based on a simple premise: Fronts and other features of interest such as Chl peaks and Chl enhancement at fronts can be revealed in satellite images by a contextual filter that removes noise but preserves the features. The second step is traditional in edge detection: since the features of interest are characterized by enhanced gradients, an edge detector, e.g. Sobel operator, would bring out these features in images that have been processed with the contextual feature-preserving filter.

2.1. Contextual median filter

The median filter (MF) is a highly efficient technique of digital filtering that removes isolated noise while preserving edges in data. When applied to a one-dimensional (1D) array, MF replaces the central value of a sliding window of an odd size by the median of sorted data from this window. When applied to an image, MF first converts each window matrix to a 1D array, then proceeds as above. This is used as a pre-processing step of other front detection algorithms (e.g. Cayula and Cornillon, 1992).

Thanks to its edge-preserving property, we have chosen MF for the first step of our front detection algorithm. At the same time, it was necessary to eliminate another – undesired – property that standard MF shares with all other digital filters; this property can be called *extremum alteration*. Indeed, standard MF always alters peaks and ridges by clipping them. In other words, standard MF degrades isolated sharp extrema and roof edges by making them blunt. This property is especially detrimental to, and therefore not acceptable in, any algorithm for feature extraction from Chl field since sharp isolated extrema (peaks) correspond to local Chl blooms, while ridges (roof edges) correspond to Chl enhancement at fronts — and both features are common in Chl fields.

To avoid extremum alteration, the digital filter must be able to recognize sharp extrema (peaks) and ridges (roof edges) – and leave them intact. In other words, the filter has to be *context-sensitive* and *selective*. The central novel idea of our median filter is that it considers a small window within a larger context; therefore this method can be called *contextual median filter*. In oceanography, the first contextual median filter was developed for automatic classification of vertical profiles; it was validated on large climatological data sets from the North Pacific (Belkin, 1986, 1991). Since vertical profiles are 1D arrays,

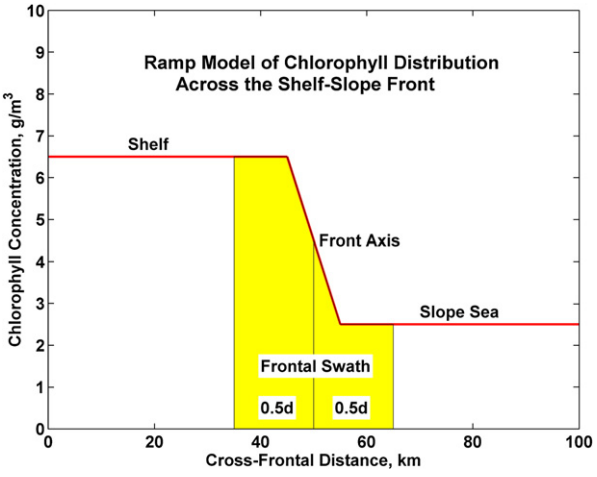

Fig. 2. Ramp model of Chl distribution across a generic shelf–slope front.

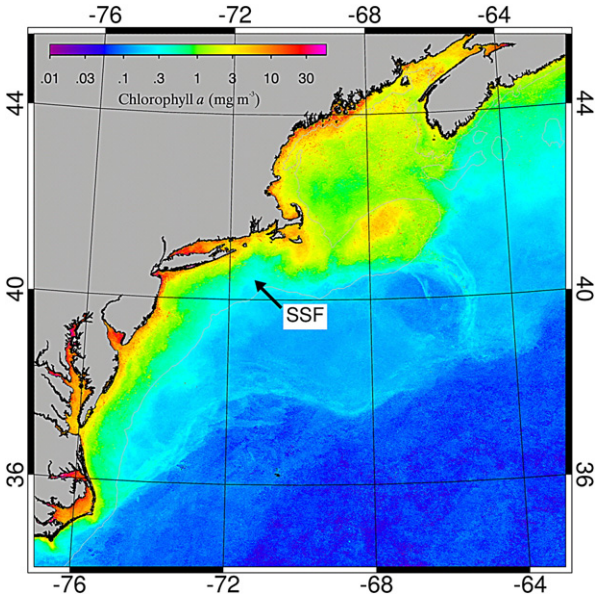

Fig. 3. Example of a stepwise change of Chl across the shelf–slope front (SSF) described by the ramp model (Fig. 2). Shown is the Chl map for the NW Atlantic from SeaWiFS data, September 2002.

all possible 1D configurations of sharp extrema were explicitly described by a set of inequalities and hard-coded into a selective MF. In our present work we used the same approach; extended it to 2D; and applied it to satellite imagery. Specifically, satellite data (Chl or SST) from a sliding 3×3-pixel window are considered within the context of a concentric 5×5-pixel window. The main problem in 2D is that there are too many possible configurations of 2D sharp extrema and roof edges to be explicitly described by a set of inequalities; this would be impractical. Instead, the contextual MF makes all possible omni-directional 1D slices across the center of a sliding 5×5-pixel 2D window; analyzes these slices; and makes a decision whether to filter the window's central pixel or leave it intact.

The above description of the algorithm is elaborated below as pseudo-code:

2.1.1. Contextual median filter (MF3in5) algorithm pseudo-code

1. Check for peaks and troughs within 1D 5-point slices through a sliding 5×5 window. The window slides east–west (E–W), north–south (N–S) across the image:

```
for I = 3:NROWS-2
    for J = 3:NCOLS-2
        Make the WE slice across the window center A(I,J);
        Make the NS slice across the window center A(I,J);
        Make the NW–SE slice across the window center A(I,J);
        Make the NE–SW slice across the window center A(I,J);
        If the window center A(I,J) is a 5-point minimum or
        maximum along all four 5-point 1D slices, flag it as Peak-5
    end
end
```

2. Check for peaks and troughs within 1D 3-point slices through sliding 3×3 window. The window slides west–east, north–south across the image:

```
for I = 3:NROWS-2
    for J = 3:NCOLS-2
        If the window center A(I,J) is a 3-point maximum or
        minimum in 2D, mark it as Peak-3
    end
end
```

3. Apply the selective 2D 3×3 median filter within sliding 3×3 window. If the window center is a significant 5-point extremum (Peak-5), leave it intact (do not blunt it with median filter), otherwise if the window center is a spike (Peak-3) use the 2D 3×3 median filter:

```
for I = 3:NROWS-2
    for J = 3:NCOLS-2
        if (Center is Peak-5) skip the 3×3 Median Filter
        elseif (Center is Peak-3)
            apply the 3×3 Median Filter
        end
    end
end
```

The above description and pseudo-code explain how contextual MF works during a single pass over a satellite image. In many applications, median filters are only applied once, as a single pass, since computational cost of *iterative* MF is often believed to be prohibitive. In reality, however, the iterative MF is quite efficient and

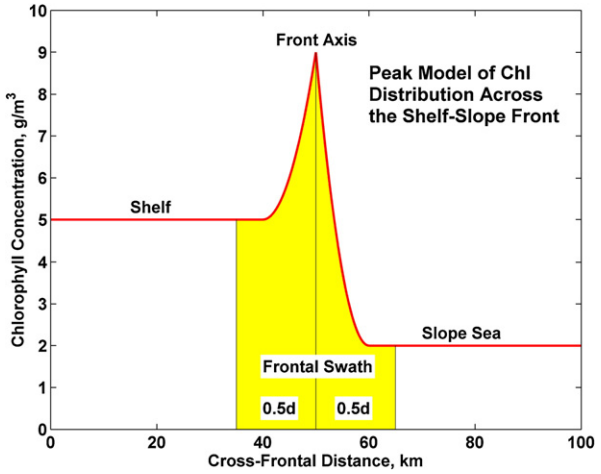

Fig. 4. Peak model of Chl distribution across a generic shelf–slope front.

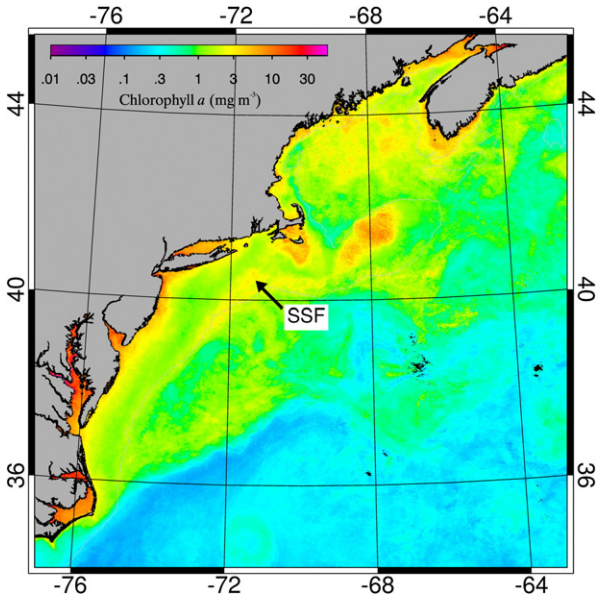

Fig. 5. Example of Chl enhancement at the shelf–slope front (SSF) described by the peak model. Shown is the Chl map for the NW Atlantic from SeaWiFS data, April 2001.

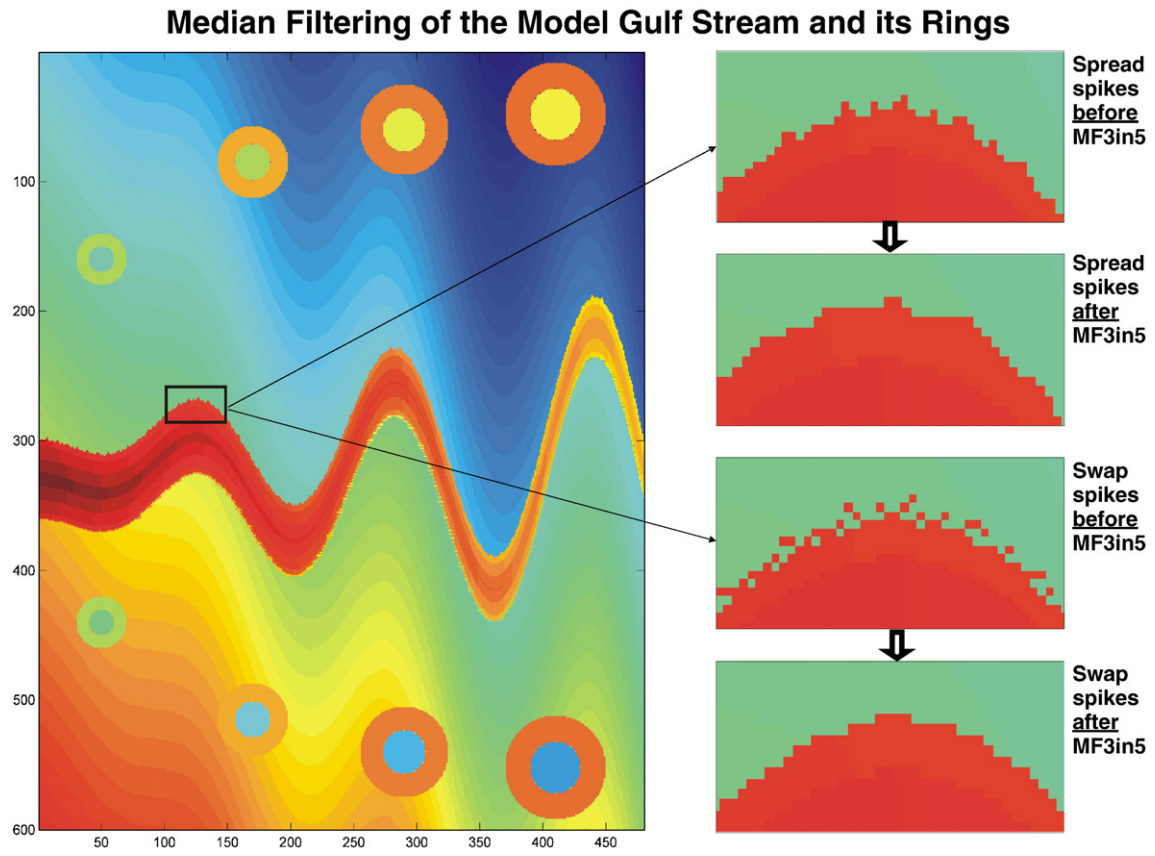

Fig. 6. Contextual median filtering of the model Gulf Stream and its rings. The model Gulf Stream's edges are frayed with horizontal spread and swap spikes. Both types of horizontal spikes and isolated vertical spikes within rings are removed by the contextual median filter MF3in5.

computationally inexpensive owing to the following properties (Gallagher and Wise, 1981):

(1) Iterative MF in 1D always converges: After a number of iterations, the next iteration does not alter the signal;
(2) Iterative MF converges to the so-called *root signal*, which is *locally monotonous* consisting of monotonous segments (ramps) and plateaus;

Iterative MF converges fast: The number of iterations until convergence, NITER, does not exceed $(N-2)/2$, where N is the number of data points in the 1D array to be filtered. Since NITER is a linear function of N, iterative MF converges much faster than most digital filters, whose convergence rate depends nonlinearly on the number of data points; typically, NITER$\sim N^2$. In our experiments with model (synthetic) images described below, MF converged after a few iterations.

2.2. Testing contextual median filter on model (synthetic) images

Performance of the contextual MF was evaluated on model (synthetic) images (Figs. 6–8) that capture main spatial features of frontal zones on a variety of scales:

1. Large-scale water mass fronts, e.g. Gulf Stream (100–1000 km).
2. Meso-scale fronts around eddies, especially rings (50–100 km).
3. Meso-to-small-scale fronts around spin-off eddies ("shingles") that develop on large-scale and meso-scale fronts (10–50 km).
4. Chl enhancement at fronts (Chl ridges).
5. Local Chl blooms (Chl peaks).

The above features were modeled against spatially varying fields to test the filter's insensitivity to the background. Testing the filter on the widely meandering Gulf Stream (GS hereafter), round-shaped rings and spiral eddies/ridges confirms the filter's rotational invariance.

The GS north and south edge ("wall") have been intentionally corrupted by adding 1-point spikes and 3-point spikes that alternate along each edge. To test the algorithm's insensitivity to spike rotation/orientation, meridionally-oriented spikes were added to the north wall, while zonally-oriented spikes were added to the south wall. Two kinds of horizontal spikes in *xy*-plane were used for testing:

1. Spikes created by *swapping* adjacent pixels. After these spikes are added, the GS edges look frayed.
2. Spikes created by *spreading* the GS warm pixels outward. After these spikes are added, the GS edges look rugged.

The swap and spread spikes make the model Gulf Stream edges mimic small- and mesoscale shingle-like meanders commonly observed along edges of the real Gulf Stream and other large-scale fronts (Fig. 6).

Rings (Fig. 6) and spiral eddies-ridges (Fig. 7) vary in size to test the filter's scale invariance and its insensitivity to feature dilation (scaling transformation). The spiral eddies-ridges also vary in structure: narrow ridges (left column) are only one pixel across, whereas wide ridges (right column) are three pixels across and have a sharp crest.

Chl peaks (blobs) are of three sizes (Fig. 8): 1-pointers are spikes assumed noise that must be removed, whereas sharp 3-pointers and 5-pointers defined on 3×3 and 5×5 compacts respectively need to be preserved intact. Since the 1-pointers are along z-axis, they are called *vertical spikes*.

2.3. Noise removal and smoothing

Since we are interested in preserving even relatively small-scale features, just a few pixels across, we do not use any smoothers, e.g. Gaussian, often used in applications elsewhere. In those applications, the

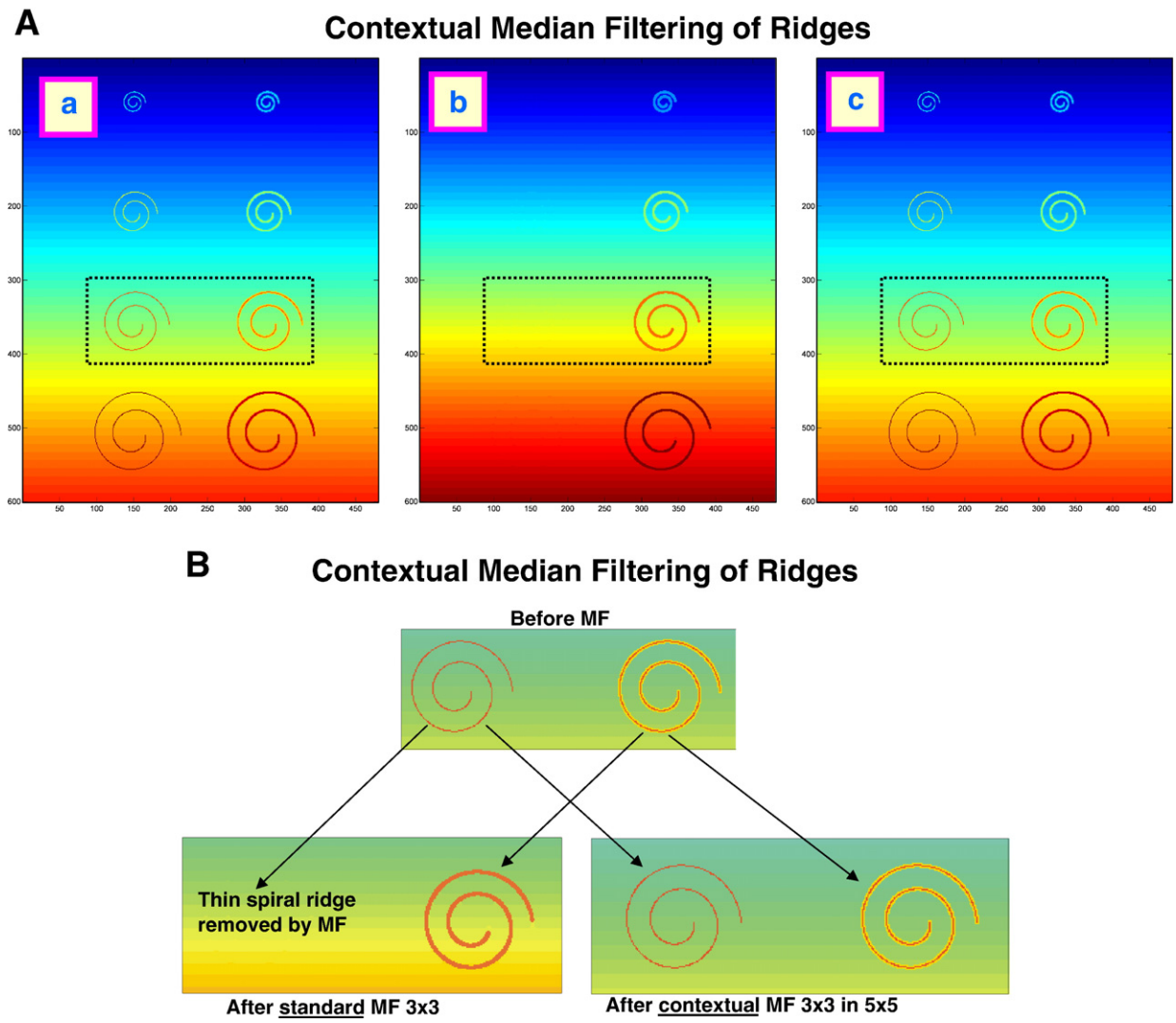

Fig. 7. A. Contextual median filtering of ridges. Thin (1-pixel wide) and wide (3-pixel wide) spiral ridges are shown before MF (a), after standard MF (b), and after contextual MF (c). Insets are enlarged in Fig. 7B. B. Contextual median filtering of ridges (enlarged insets from Fig. 7A). Thin (1-pixel wide) and wide (3-pixel wide) spiral ridges (top panel) are processed with standard MF (left) and the contextual MF3in5 (right). Standard MF removes thin ridge and blunts the crest of wide ridge (bottom left panel). Contextual MF3in5 does not alter either ridge, thereby preserving intact both ridges (bottom right panel).

signal (object) has a substantially larger scale, which is typically at least an order of magnitude larger than the noise; therefore a smoothing operator might improve the object's visibility in the image. In our case, the signal-to-noise scale ratio can be as small as 3, e.g. 3-pixel Chl peaks versus 1-pixel spikes. Therefore, in our situation, any smoothing could be detrimental to gradient computation and climatology of relatively small but biologically important features in Chl field.

2.4. Gradient computation

The gradient vector is computed by the Sobel operator consisting of two 3×3 convolution masks or kernels: $GX = [-1\,0\,+1; -2\,0\,+2; -1\,0\,+1]$; and $GY = [+1\,+2\,+1; 0\,0\,0; -1\,-2\,-1]$; GY is simply GX rotated 90 degrees counter-clockwise. These kernels are used to calculate two images, Gx and Gy respectively, containing approximations for derivates in X and Y directions. If A is the original image, then $Gx = GX*A$ and $Gy = GY*A$, where * is the convolution sign. At each point of the image, gradient magnitude and direction are computed as $GM = \mathrm{sqrt}(Gx^2 + Gy^2)$ and $GD = \arctan(Gy/Gx)$ respectively. The Sobel operator is known as a simple and effective way of enhancing visibility of edges in digital images and is widely used in a variety of applications, partly owing to its ultimate simplicity.

2.5. Gradient mapping: log-transformation of Chl data

Chlorophyll distribution on the global scale is approximately log-normal (Campbell, 1995). Therefore Chl data are usually log-normally transformed before any processing, mapping and statistical evaluation (e.g. Gregg and Conkright, 2001; Gregg and Casey, 2004). We have computed global Chl distribution from SeaWiFS, 1997–2007 (not shown) to confirm earlier findings based on spatially limited or irregular data (e.g. Campbell, 1995). We have also found a similar log-normal distribution in our study area (not shown) which encompasses shelf, slope and Sargasso Sea water and the three-orders-of-magnitude range in surface Chl. Therefore we have *log-normally transformed* original Chl data and calculated Chl gradient from the log-normally transformed data. Our *logarithmic gradient* of Chl at every pixel is the difference between natural logarithms of Chl at adjacent pixels that is the natural *logarithm of the ratio* of adjacent Chl values.

3. Front detection in real satellite images

The algorithm was thoroughly tested on real satellite images that cover the Northeast U.S. Continental Shelf Large Marine Ecosystem (Fig. 9). Two examples of synoptic frontal maps for Chl and SST are

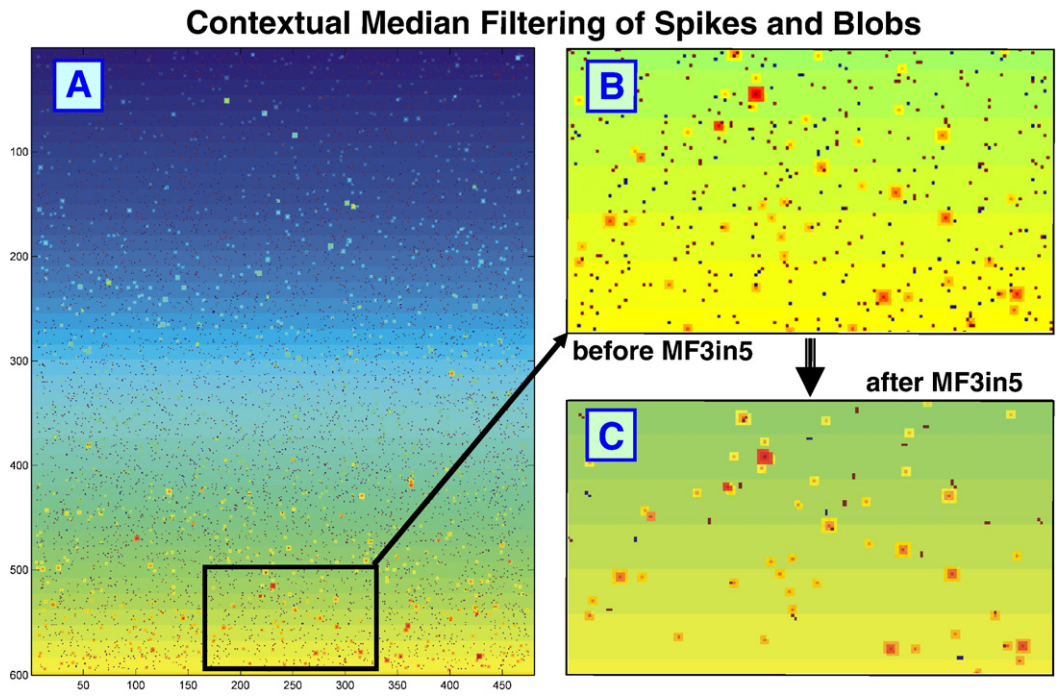

Fig. 8. Contextual median filtering of spikes and blobs. The inset in the original test image A is enlarged and shown before (B) and after (C) the entire image is processed with the contextual median filter MF3in5 that completely removes ordinary spikes (black 1-pixel specs in B) but preserves sharp 3- and 5-point peaks (yellow and orange specs in C) that may represent localized point-wise chlorophyll blooms.

presented in Fig. 10. After testing on selected synoptic images, the algorithm was used to generate over 6000 daily frontal maps for the Mid-Atlantic Bight and the greater Northwest Atlantic area, from 1997–2007, for Chl and SST. These synoptic (instant) maps reveal a complex pattern of fronts on a variety of scales, from O(1000 km) down to the satellite data resolution, O(1 km). The smaller scales, between O(10 km) and O(1 km), remain virtually unexplored. And yet, these smaller scales may well be critical for physical–biological interactions. To most species that live far from large-scale fronts, the sub-mesoscale range, O(1–10 km), is the only scale that matters, and now we resolve this scale. It is also important to observe directly abrupt changes of dominant frontal scales from one region to another (Fig. 10). Indeed, the dominant scale over Georges Bank is very small compared to that in the Gulf of Maine; the latter, in turn, being markedly smaller than the dominant scale in the Slope Sea and south of the Gulf Stream. These scales are expected to change as the season progresses, and they also may change interannually; we plan to investigate these processes quantitatively from satellite data.

4. Discussion

The newly available satellite frontal data base generated with the new algorithm opens an unprecedented opportunity to study quantitatively spatial and temporal relationships between Chl and SST fronts using an automatic, objective method. One of the most interesting problems in this respect is the spatial offset between SST and Chl fronts (e.g. Stegmann and Ullman, 2004). This problem has barely been touched upon; high-resolution ground truth *in situ* observations are necessary to quantify the Chl–SST cross-frontal offset and its seasonal variability.

Another important application of the new algorithm is a general-purpose frontal tracking and mapping. It is well known that even large-scale thermal fronts like the Gulf Stream and Kuroshio all but disappear at the sea surface in summer; their surface manifestation being almost completely obliterated by summer warming that acts to decrease spatial contrasts across thermal fronts by creating a thin, spatially uniform upper layer that masks the fronts. Fortunately, these fronts can be detected from the Chl field. In many instances, frontal visibility in the Chl field actually *improves in summer* as can be seen, for example, from frontal maps in Section 3, where the Gulf Stream "north wall" is much better delineated in Chl field vs. SST, in summer. Similar observations have been made in the NW Pacific where the Kuroshio Front can be reliably detected from Chl field in summer when the front's thermal manifestation disappears (Takahashi and Kawamura, 2005; the Kuroshio Front's summertime disappearance in SST field has been noted by Hickox et al., 2000). In the Gulf of Mexico,

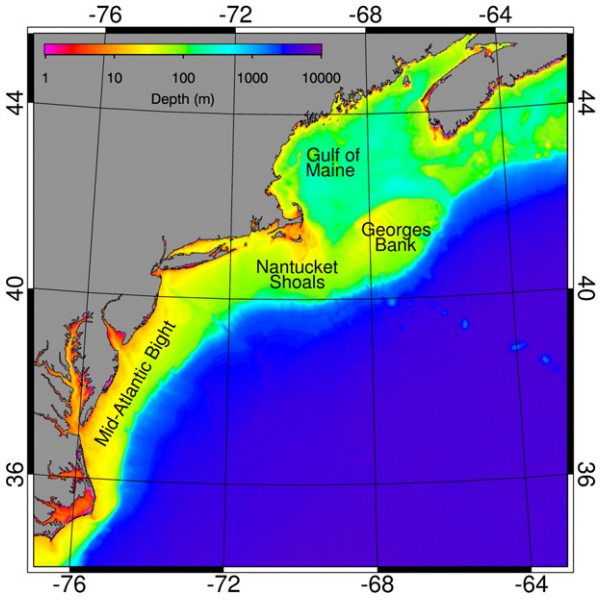

Fig. 9. Base map of the study area.

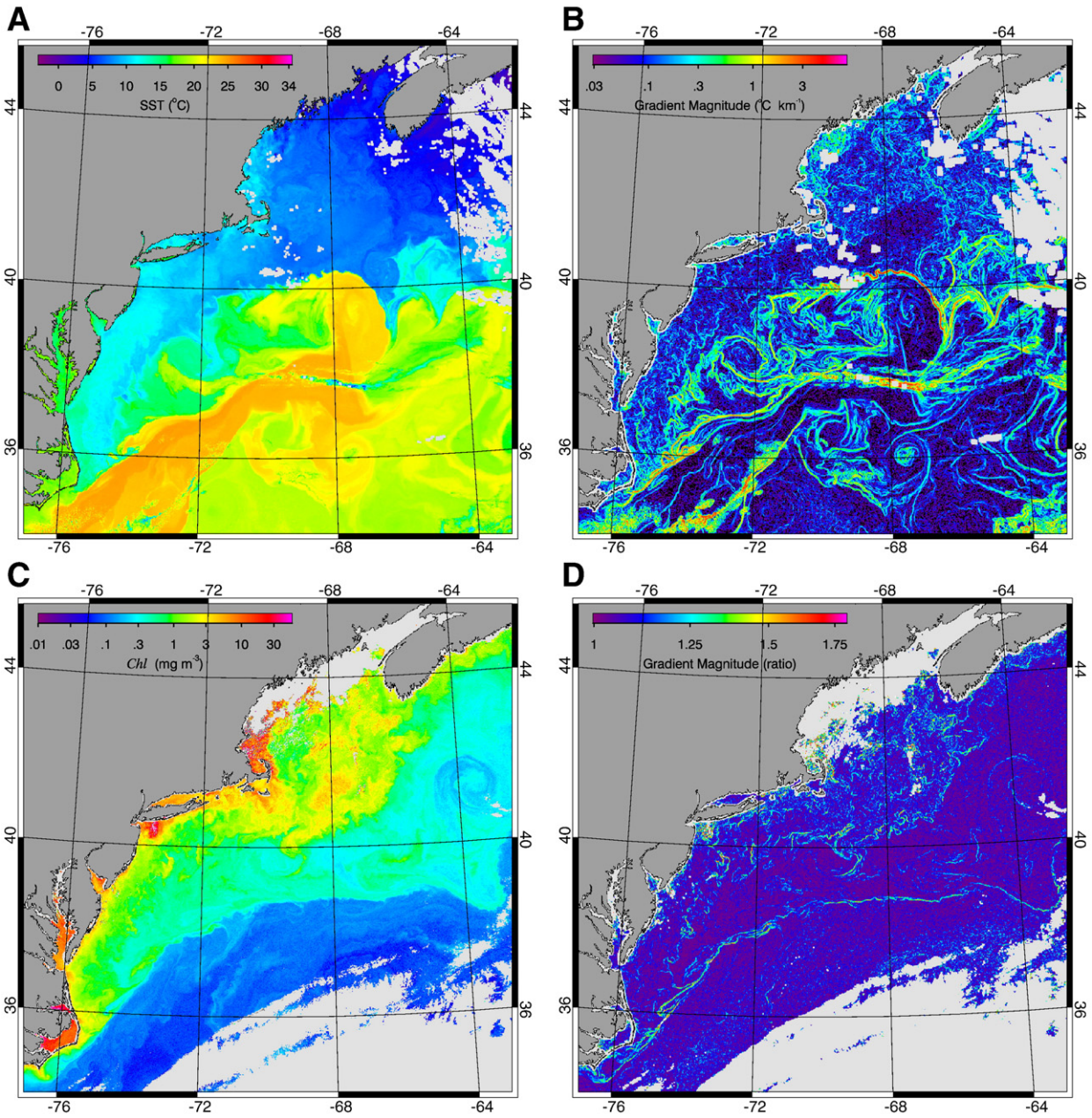

Fig. 10. Examples of the algorithm performance on synoptic satellite images of SST (top row; 3 May 2001) and chlorophyll (bottom row; 14 October 2000). Left column, original images. Right column, gradient magnitude.

Legeckis et al. (2002) used Chl to map the Loop Current Front in summer (June–October) when the front's SST signature vanishes due to seasonal heating of surface layer. Thus, an optimum front tracking system should rely on both observables, SST and Chl, and it should emphasize the importance of Chl front mapping in summer. Besides SST and Chl, such a system could also use sea surface height data from satellite altimeters.

5. Summary

In this work, a new front detection algorithm is described based on a contextual median filter that removes impulse noise (spikes) in satellite imagery and preserves important oceanographic features of chlorophyll field such as peaks (localized blooms) and ridges (chlorophyll enhancement at hydrographic fronts) in addition to steps and ramps typical for SST fronts. The algorithm is tested first on model (synthetic) images and then on 6000 real synoptic images from 1997–2007, both Chl and SST, by producing frontal climatologies for the Mid-Atlantic Bight and a greater Northwest Atlantic; these results are presented in detail elsewhere (Belkin, I.M., J.E. O'Reilly, K.J.W. Hyde, and T. Ducas (2008) Satellite climatologies of chlorophyll and SST fronts off the U.S. Northeast, *Progress in Oceanography*, in Belkin et al., in preparation). These frontal climatologies document spatial, seasonal and interannual variability of large-scale fronts associated with major western-boundary currents such as the Gulf Stream, North Atlantic Current, and Labrador Current; water mass fronts such as the Shelf–Slope Front; tidal mixing fronts around Georges Bank and Gulf of Maine; and fronts associated with buoyancy-driven coastal jets due to river discharge. Substantially different frontal scales are found to dominate certain regions, e.g. Gulf of Maine and Georges Bank. Owing to the algorithm's feature preservation and MODIS imagery's high resolution, small-to-mesoscale (O(1 km) to O(10 km)) fronts can be reliably detected and statistically studied from remote sensing data.

Acknowledgments

This project was funded by NOAA under the "Research to Operations" program and through a contract to the University of Rhode Island. We are grateful to Kimberly Hyde for testing our algorithm in the Northeast U.S. continental waters and for providing Figs. 5 and 10, and to Teresa Ducas for her extensive assistance with computer programming and analysis of satellite data. The original manuscript has been significantly improved thanks to numerous comments made by seven anonymous reviewers and alternative guest editor, Peter Miller.

References

Belkin, I.M., 1986. Morpho-statistical objective classification of vertical profiles of hydrophysical parameters. Transanctions of the Academy of Sciences of the USSR 286 (3), 707–711.
Belkin, I.M., 1991. Morpho-Statistical Analysis of Ocean Stratification [Morfologo-Statisticheskii Analiz Stratifikatsii Okeana]. Gidrometeoizdat, Leningrad. 134 pp. (in Russian).
Belkin, I.M., Cornillon, P.C., 2003. SST fronts of the Pacific coastal and marginal seas. Pacific Oceanography 1 (2), 90–113.
Belkin, I.M., Cornillon, P.C., 2004. Surface thermal fronts of the Okhotsk Sea. Pacific Oceanography 2 (1–2), 6–19.
Belkin, I.M., Cornillon, P.C., 2005. Bering Sea thermal fronts from Pathfinder data: seasonal and interannual variability. Pacific Oceanography 3 (1), 6–20.
Belkin, I.M., Shan, Z., Cornillon, P., 1998. Global survey of oceanic fronts from Pathfinder SST and in-situ data. AGU 1998 fall meeting abstracts. Eos 79 (45, Suppl.), F475.
Belkin, I.M., Cornillon, P., Shan, Z., 2001. Global survey of ocean fronts from Pathfinder SST data. Abstracts of the Oceanography Society Meeting, April 2–5, 2001, Miami Beach, FL. Oceanography, vol. 14 (1), p. 10.
Belkin, I.M., Cornillon, P.C., Ullman, D., 2003. Ocean fronts around Alaska from satellite SST data. Proceedings of the American Meteorological Society 7th Conference on the Polar Meteorology and Oceanography, Hyannis, MA, Paper 12.7. 15 pp.
Belkin, I.M., Cornillon, P.C., Sherman, K., 2009. Fronts in Large Marine Ecosystems. Progress in Oceanography 81 (1-4), 223–236. doi:10.1016/j.pocean.2009.04.015.
Belkin, I.M., Hyde, K.J.W., O'Reilly, J.E., Ducas, T., in preparation. Satellite climatologies of chlorophyll and SST fronts off the U.S. East Coast.
Bontempi, P.S., Yoder, J.A., 2004. Spatial variability in SeaWiFS imagery of the South Atlantic bight as evidenced by gradients (fronts) in chlorophyll *a* and water-leaving radiance. Deep-Sea Research II 51 (10–11), 1019–1032.
Breaker, L.C., Mavor, T.P., Broenkow, W.W., 2005. Mapping and monitoring large-scale ocean fronts off the California Coast using imagery from GOES-10 geostationary satellite. Publication T-056, California Sea Grant College Program, University of California, San Diego. 25 pp., http://repositories.cdlib.org/csgc/rcr/Coastal05_02.
Campbell, J.W., 1995. The lognormal distribution as a model for bio-optical variability in the sea. Journal of Geophysical Research 100 (C7), 13237–13254.
Canny, J.F., 1986. A computational approach to edge detection. IEEE Transactions on Pattern Analysis and Machine Intelligence 8 (6), 679–698.
Castelao, R.M., Mavor, T.P., Barth, J.A., Breaker, L.C., 2006. Sea surface temperature fronts in the California Current System from geostationary satellite observations. Journal of Geophysical Research 111, C09026. doi:10.1029/2006JC003541.
Cayula, J.-F., Cornillon, P., 1992. Edge detection algorithm for SST images. Journal of Atmospheric and Oceanic Technology 9 (1), 67–80.
Cayula, J.-F., Cornillon, P., 1995. Multi-image edge detection for SST images. Journal of Atmospheric and Oceanic Technology 12 (4), 821–829.
Cayula, J.-F., Cornillon, P., 1996. Cloud detection from a sequence of SST images. Remote Sensing of Environment 55 (1), 80–88.
Cayula, J.-F., Cornillon, P., Holyer, R., Peckinpaugh, S., 1991. Comparative study of two recent edge-detection algorithms designed to process sea-surface temperature fields. IEEE Transactions on Geoscience and Remote Sensing 29 (1), 175–177.
Chan, C.O., 1999. Spatial patterns in ocean color and temperature maps: fronts, fractals and ecological considerations. Ph.D. Thesis, Graduate School of Oceanography, University of Rhode Island, Narragansett, RI, 173 pp.
Gallagher, N.C., Wise, G.L., 1981. A theoretical analysis of the properties of median filters. IEEE Transactions on Acoustics. Speech and Signal Processing ASSP-29, vol. (6), pp. 1136–1141.
Gregg, W.W., Conkright, M.E., 2001. Global seasonal climatologies of ocean chlorophyll: blending in situ and satellite data for the Coastal Zone Color Scanner era. Journal of Geophysical Research 106 (2), 2499–2515.
Gregg, W.W., Casey, N.W., 2004. Global and regional evaluation of the SeaWiFS chlorophyll data set. Remote Sensing of Environment 93 (4), 463–479.
Hickox, R., Belkin, I.M., Cornillon, P.C., Shan, Z., 2000. Climatology and seasonal variability of ocean fronts in the East China, Yellow and Bohai Seas from satellite SST data. Geophysical Research Letters 27 (18), 2945–2948.
Holyer, R.J., Peckinpaugh, S.H., 1989. Edge detection applied to satellite imagery of the oceans. IEEE Transactions on Geoscience and Remote Sensing 27 (1), 46–56.
Kahru, M., Hkansson, B., Rud, O., 1995. Distributions of the sea-surface temperature fronts in the Baltic Sea as derived from satellite imagery. Continental Shelf Research 15 (6), 663–679.
Kazmin, A.S., Rienecker, M.M., 1996. Variability and frontogenesis in the large-scale oceanic frontal zones. Journal of Geophysical Research 101 (C1), 907–921.
Kostianoy, A.G., Ginzburg, A.I., Frankignoul, M., Delille, B., 2004. Fronts in the southern Indian Ocean as inferred from satellite sea surface temperature data. Journal of Marine Systems 45 (1–2), 55–73.
Legeckis, R., 1978. A survey of worldwide sea surface temperature fronts detected by environmental satellites. Journal of Geophysical Research 83 (C9), 4501–4522.
Legeckis, R., Christopher, W.B., Chang, P.S., 2002. Geostationary satellites reveal motions of ocean surface fronts. Journal of Marine Systems 37 (1–3), 3–15.
Marra, J., Houghton, R.W., Garside, C., 1990. Phytoplankton growth at the shelf-break front in the Middle Atlantic Bight. Journal of Marine Research 48 (4), 851–868.
Mavor, P.T., Bisagni, J.J., 2001. Seasonal variability of sea-surface temperature fronts on Georges Bank. Deep-Sea Research II 48 (1–3), 215–243.
Miller, P.I., 2004. Multi-spectral front maps for automatic detection of ocean colour features from SeaWiFS. International Journal of Remote Sensing 25 (7–8), 1437–1442.
Miller, P.I., 2009. Composite front maps for improved visibility of dynamic sea-surface features on cloudy SeaWiFS and AVHRR data. Journal of Marine Systems 78 (3), 327–336 (this issue).
Moore, J.K., Abbott, M.R., Richman, J.G., 1997. Variability in the location of the Antarctic Polar Front (90°–20°W) from satellite sea surface temperature data. Journal of Geophysical Research 102 (C13), 27,825–27,834.
Moore, J.K., Abbott, M.R., Richman, J.G., 1999. Location and dynamics of the Antarctic Polar Front from satellite sea surface temperature data. Journal of Geophysical Research 104 (C2), 3059–3074.
Nieto, K., Demarcq, H., 2006. Multi-image edge detection on SST and chlorophyll satellite images in northern Chile. Workshop on Indices of Mesoscale Structures, 22–24 February 2006, IFREMER, Nantes, France. www.ices.dk/reports/occ/2006/wkims06.pdf.
Ryan, J.P., Yoder, J.A., Cornillon, P.C., 1999a. Enhanced chlorophyll at the shelfbreak of the Mid-Atlantic Bight and Georges Bank during the spring transition. Limnology and Oceanography 44 (1), 1–11.
Ryan, J.P., Yoder, J.A., Cornillon, P.C., Barth, J.A., 1999b. Chlorophyll enhancement and mixing associated with meanders of the shelf break front in the Mid-Atlantic Bight. Journal of Geophysical Research 104 (C10), 23479–23493.
Shimada, T., Sakaida, F., Kawamura, H., Okumura, T., 2005. Application of an edge detection method to satellite images for distinguishing sea surface temperature fronts near the Japanese coast. Remote Sensing of Environment 98 (1), 21–34.
Stegmann, P.M., Ullman, D.S., 2004. Variability in chlorophyll and sea surface temperature fronts in the Long Island Sound outflow region from satellite observations. Journal of Geophysical Research 109, C07S03. doi:10.1029/2003JC001984.
Takahashi, W., Kawamura, H., 2005. Detection method of the Kuroshio front using the satellite-derived chlorophyll-a images. Remote Sensing of Environment 97 (1), 83–91.
Ullman, D.S., Cornillon, P.C., 1999. Surface temperature fronts off the East Coast of North America from AVHRR imagery. Journal of Geophysical Research 104 (C10), 23459–23478.
Ullman, D.S., Cornillon, P.C., 2000. Evaluation of front detection methods for satellite-derived SST data using in situ observations. Journal of Atmospheric and Oceanic Technology 17 (12), 1667–1675.
Ullman, D.S., Cornillon, P.C., 2001. Continental shelf surface thermal fronts in winter off the northeast US coast. Continental Shelf Research 21 (11–12), 1139–1156.
Vazquez, J., Perry, K., Kilpatrick, K., 1998. NOAA/NASA AVHRR Oceans Pathfinder Sea Surface Temperature Data Set User's Reference Manual, Version 4.0. JPL Publication D-14070. http://podaac.jpl.nasa.gov/pub/sea_surface_temperature/avhrr/pathfinder/doc/usr_gde4_0.html.
Vazquez, D.P., Atae-Allah, C., Luque-Escamilla, P.L., 1999. Entropic approach to edge detection for SST images. Journal of Atmospheric and Oceanic Technology 16 (7), 970–979.